Volume 15
Number 25
7 July 2024
Pages 2531-2620

Polymer Chemistry

rsc.li/polymers

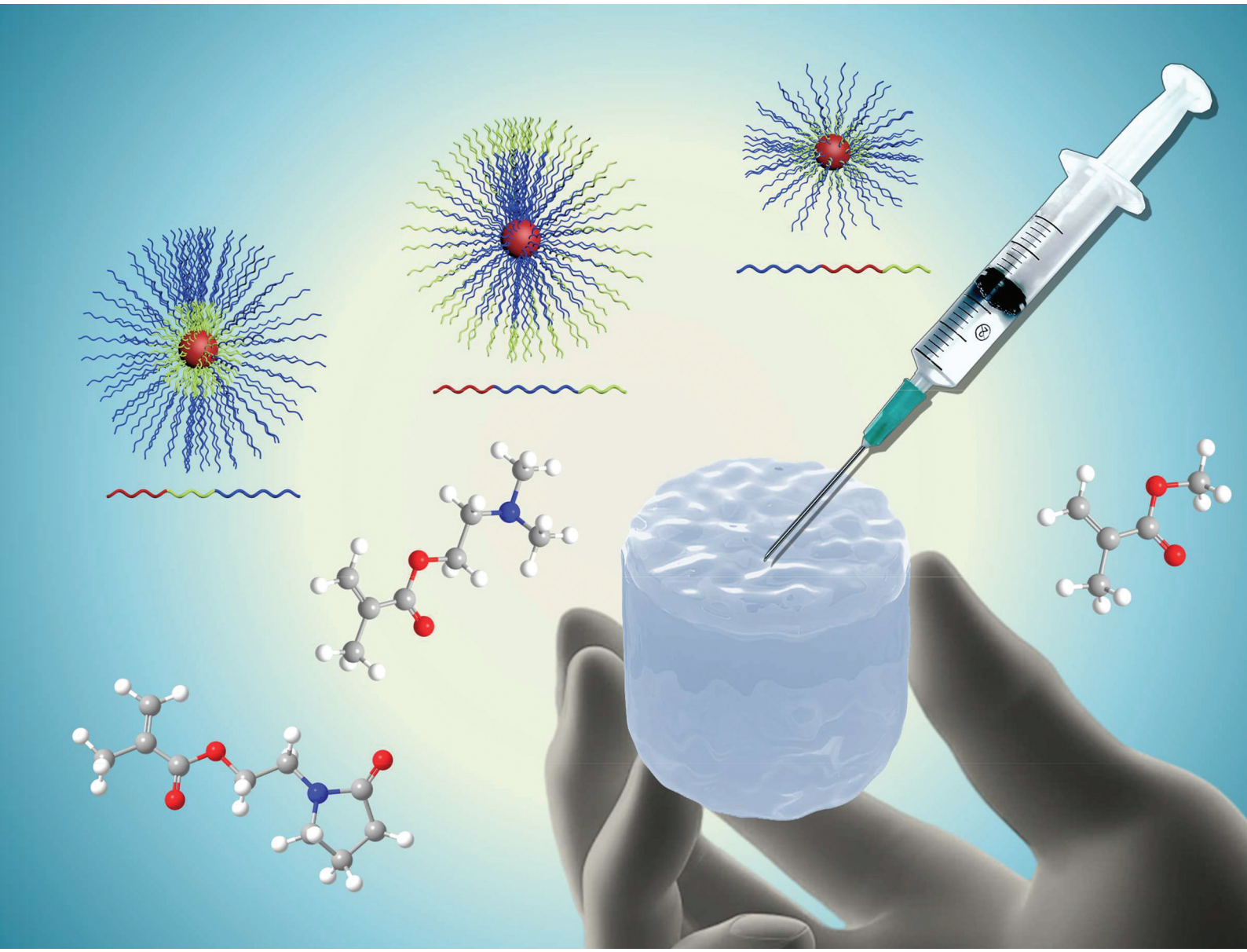

ISSN 1759-9962

ROYAL SOCIETY OF CHEMISTRY

PAPER
Theoni K. Georgiou *et al.*
Influence of architectural design on the thermoresponsive properties of pyrrolidone-based terpolymers

Polymer Chemistry

ROYAL SOCIETY OF CHEMISTRY

PAPER

View Article Online
View Journal | View Issue

Open Access Article. Published on 07 June 2024. Downloaded on 6/20/2025 10:30:49 AM.
This article is licensed under a Creative Commons Attribution 3.0 Unported Licence.

Check for updates

Cite this: *Polym. Chem.*, 2024, **15**, 2548

Influence of architectural design on the thermoresponsive properties of pyrrolidone-based terpolymers†

Lezhi Wang, Haffsah Iqbal and Theoni K. Georgiou *

Received 13th April 2024,
Accepted 23rd May 2024

DOI: 10.1039/d4py00405a

rsc.li/polymers

This study investigated a new series of amphiphilic, thermoresponsive terpolymers based on pyrrolidone. The terpolymers feature similar compositions and molar masses but differ in their architectures, *i.e.*, the position of comonomers along the polymer chain. All polymers were synthesised *via* reversible addition–fragmentation chain transfer (RAFT) polymerisation. The study focused on the polymers' thermoresponsive behaviour in aqueous solutions. Specifically, the cloud point temperatures (T_{cp}) and self-assembly conformations, as well as the thermally induced sol–gel transitions, were investigated. The terpolymers exhibit a solvent isotropic effect and display different T_{cp}s in deuterium oxide (D_2O) and deionised water (H_2O), as determined through turbidimetry measurements. The phase transitions were further analysed using temperature-variation ^{1}H NMR spectroscopy. Dynamic light scattering and transmission electron microscopy revealed that the triblock structure could self-assemble into micelles, whereas the statistical polymer could not. The micelle size varied depending on the pH. Visual testing and rheological studies showed how the polymer architecture influences thermoresponsive behaviour, with the BAC architecture exhibiting the widest gelation window. This research illustrates the importance of structure–property relationships and highlights the critical role of polymer architecture in their self-assembly and thermoresponsive properties.

1. Introduction

Polymers capable of undergoing a reversible phase transition in structure or solubility in response to changes in external stimuli, such as temperature,[1–3] pH,[4,5] light,[6–8] and electrical or magnetic fields,[9,10] are termed 'smart polymers'. These polymers have attracted significant attention in fundamental research due to their diverse applications. Among the various stimuli-responsive polymers, thermo- and pH-responsive polymers are of particular interest, especially for their potential roles in the biomedical and pharmaceutical sectors, including the controlled delivery of proteins and drugs.[11–13]

A prime example of such a polymer is poly[(2-dimethyl amino)ethyl methacrylate] (PDMAEMA), which exhibits responsiveness to both pH and temperature.[14–16] At a pH of 8.5, this polymer has a lower critical solution temperature (LCST) of around 45 °C.[17] In aqueous settings, its pK_a lies between 7.3–7.5.[18] PDMAEMA features a pendant side group that has a tertiary amine structure. By altering the pH of its environment, PDMAEMA can undergo protonation, becoming more hydrophilic and cationic at low pH levels, while deprotonation at elevated pH levels increases its hydrophobicity.[19] The pH sensitivity of PDMAEMA-based hydrogels affects their volume phase transition behaviour near the LCST, a phenomenon attributed to the formation and disruption of hydrogen bonds between the tertiary amine group and water molecules under varying pH conditions.[20,21] It has been observed that protonated PDMAEMA hydrogels display increased hydrophilicity and significant swelling in acidic environments, while in basic conditions, they dehydrate and contract.[22–24] Thus, the dual responsiveness of PDMAEMA hydrogels to temperature and pH renders them ideal for diverse applications, such as drug delivery,[25] contact lenses,[26] and biosensors.[27]

Another promising category of polymers, which exhibits dual responsiveness in the biomedical domain, is the pyrrolidone-based polymers. Their notable biocompatibility, water solubility, and coordination capacity stem from the pyrrolidone group, which also imparts pH sensitivity to the polymer due to its amine group that can be protonated under acidic conditions.[28,29] A renowned pyrrolidone-based polymer, poly(*N*-vinyl pyrrolidone) (PNVP), is utilised in medical devices and pharmaceutical applications due to its biocompatibility.[30,31] However, synthesising PNVP poses challenges as NVP, its monomer, is less reactive, especially for the conventional reversible addition–fragmentation chain transfer (RAFT) polymerisation.[32] Research indicates that synthesising PNVP polymers requires a careful choice of RAFT agents to ensure optimal reaction control.[33,34]

Department of Materials, Imperial College London, Exhibition Road, SW7 2AZ London, UK. E-mail: t.georgiou@imperial.ac.uk

† Electronic supplementary information (ESI) available. See DOI: https://doi.org/10.1039/d4py00405a

This journal is © The Royal Society of Chemistry 2024

Open Access Article. Published on 07 June 2024. Downloaded on 6/20/2025 10:30:49 AM. This article is licensed under a Creative Commons Attribution 3.0 Unported Licence.

To address this challenge, researchers have turned to *N*-(2-methacryloyloxy)ethyl pyrrolidone (NMEP) as a superior alternative to NVP due to its versatility and ease of synthesis. Unlike NVP, NMEP's polymerisable group is a methacrylate. This characteristic facilitates more straightforward re-initiation with acrylamides, acrylates, and other methacrylates using controlled polymerisation techniques, such as RAFT and atom transfer radical polymerisation (ATRP).[35] Notably, Davis and his team successfully synthesised a series of pyrrolidone-based homopolymers with different side chain lengths using free radical polymerisations, showcasing their thermoresponsive attributes.[36] Cai's group further refined PNMEP samples using visible light-activated RAFT polymerisation.[37,38] They accurately determined the cloud points (T_{cp}s) for PNMEP, which ranged from 71.5 °C to 52.8 °C as the molar mass (MM) increased from 20.6 kg mol^{-1} to 105.4 kg mol^{-1}. This observed LCST range was subsequently verified by Armes's group.[39] They employed RAFT solution polymerisation method and identified an LCST of 55 °C with a MM of around 100 kg mol^{-1}. Additionally, Gibson *et al.*, utilising a carboxylic acid-functional RAFT agent in ethanol, again through the RAFT solution polymerisation technique, produced PNMEP polymers with a pK_a that was measured between 5.07 and 5.44.[40]

Researchers have exploited the stimuli-responsive capabilities of NMEP-based polymeric systems to harness a wide array of their applications in the biomedical field. Teunissen *et al.* developed thermoresponsive diblock copolymer brushes based on PNMEP using surface-initiated atom transfer radical polymerisation, showcasing their suitability for biomedical applications due to their exceptional antifouling characteristics and temperature-responsive behaviour.[41,42] In a separate study, Magalhães *et al.* synthesised flexible and biocompatible hydrogels by combining NMEP with hyaluronic acid (HA), underscoring the potential of PNMEP-HA hydrogels in drug delivery systems tailored to the body's internal pH variations.[43] Jia *et al.* employed an amphiphilic diblock copolymer composed of PNMEP to anchor haemoglobin, achieving impressive protein loading and maintaining bioactivity. This points to potential uses in biosensors and bioreactors.[44] Additionally, Cheng *et al.* unveiled a novel pyrrolidone-based amphiphilic diblock copolymer consisting of PNMEP and poly(methyl methacrylate) (PMMA). Upon self-assembly in isopropanol, this polymer formed thermoresponsive organogels with 3D micellar networks, hinting at potential applications in transdermal drug delivery and nanomaterials.[45]

Herein, a series of terpolymers featuring novel combinations of comonomers was synthesised *via* RAFT polymerisation, harnessing the dual-responsive properties of DMAEMA and NMEP. Previous research explored DMAEMA-MMA copolymers in both diblock and statistical architectures, revealing that only the diblock copolymer, with a MM of 31 900 g mol^{-1}, was able to form a thermoresponsive gel.[46] Consequently, this study introduced an extra block and investigated the gelation properties of terpolymers, focusing on those comprising DMAEMA (A block), MMA (B block), and NMEP (C block), arranged in various architectural arrangements—ABC, BAC, BCA, and statistical—with similar MMs and compositions. Both PDMAEMA and PNMEP exhibited thermoresponsive behaviour and weak cationic polyelectrolyte characteristics, while PMMA was chosen as the non-ionic hydrophobic component due to its extensive use in biomedical devices. The thermal transitions and self-assembly behaviour of these terpolymers were explored. Special emphasis was placed on how the position of the blocks, *i.e.* architecture, affects the formation of thermogels.

2. Experimental

2.1 Materials

1-(2-Hydroxyethyl)-2-pyrrolidone (MM = 129.16 g mol^{-1}, 98%), methacryloyl chloride (MM = 104.54 g mol^{-1}, 97%), DMAEMA (MM = 157.21 g mol^{-1}, 98%), MMA (MM = 100.12 g mol^{-1}, 99%), 2-cyano-2-propyl benzodithioate (CPDB, >97%, employed as the chain transfer agent (CTA) for RAFT polymerisation), 2,2′-azobis(2-methylpropionitrile) (AIBN, 98%, free radical initiator), 1,4-dioxane (99.8%, anhydrous), and *N*,*N*-dimethylformamide (DMF, HPLC grade ≥99.9% and anhydrous ≥99.8%) were procured from Sigma-Aldrich, UK. Sodium carbonate (Na_2CO_3, ≥98%, purified), sodium chloride (NaCl, ≥99%, purified), magnesium sulphate ($MgSO_4$, ≥98.0%, anhydrous) and *n*-hexane (≥97%, HPLC grade) were obtained from VMR Chemicals. Triethylamine (99%, anhydrous) was purchased from Fluorochem. Lithium Bromide (LiBr, 99%, purified), chloroform (99%, anhydrous), diethyl ether (≥99%, HPLC grade), and polytetrafluoroethylene (PTFE) hydrophilic syringe filters (0.45 μm pore size, 25 mm diameter) were sourced from Thermo Fisher Scientific. The deionised water was produced using the ELGA Purelab Option Water Purification System. The SEC calibration standards, PMMA samples with molecular masses (MM) of 0.54, 1.09, 1.81, 7.20, 13.90, 30.78, 72.80, 146.50, 260.90, 538.50, 1020.00, and 2210.00 kg mol^{-1}, were purchased from Agilent Technologies.

In addition to the above, other chemicals essential for the monomer and solvent purification, as well as polymer characterisation, were also acquired from Sigma-Aldrich, UK. These include calcium hydride (CaH_2, ≥97%, drying agent), basic aluminum oxide (Al_2O_3·KOH), 2,2-diphenyl-1-picrylhydrazyl hydrate (DPPH), deuterated chloroform ($CDCl_3$, 99.8%), phosphate-buffered saline (PBS, tablets, pH = 7.4 at 25 °C), sodium hydroxide pellets (NaOH, 97%) and hydrochloric acid solution (volumetric, 1 M).

2.2 Synthesis of *N*-(2-(methacryloyloxy)ethyl) pyrrolidone (NMEP) monomer

N-(2-(Methacryloyloxy)ethyl) pyrrolidone (NMEP) was *in-house* synthesised *via* the reaction between 1-(2-hydroxyethyl)-2-pyrrolidone and methacryloyl chloride. This procedure has been documented in previous studies.[36,38,47–49] Specifically, 1-(2-hydroxyethyl)-2-pyrrolidone (114.3 g, 0.89 mol), anhydrous triethylamine (179.1 g, 1.77 mol), and 400 mL anhydrous chloroform were added into a 2L dried round-bottom flask. The reac-

Open Access Article. Published on 07 June 2024. Downloaded on 6/20/2025 10:30:49 AM. This article is licensed under a Creative Commons Attribution 3.0 Unported Licence.

tion flask was then immersed in a thermostatic ice bath at 0 °C. A solution of methacryloyl chloride (120.3 g, 1.15 mol) diluted in 100 mL of anhydrous chloroform was added dropwise to the flask over a period of 2 hours. The mixture was stirred, allowed to return to room temperature, and reacted overnight.

Upon completion of the reaction, the white ammonium salt was removed through filtration. The remaining solution was concentrated using rotary evaporation and extracted with a 5% Na_2CO_3 solution, followed by a saturated NaCl solution. The mixture was then dried under anhydrous $MgSO_4$ and filtered. It was then passed through basic alumina and distilled under reduced pressure to yield the purified target monomer. The successful synthesis of the monomer was verified using ^{1}H NMR (δ, in $CDCl_3$). δ 6.01 (m, 1H, C**H**$_2$=C(CH$_3$)–), δ. 5.49 (m, 1H, C**H**$_2$=C(CH$_3$)–), δ 4.18 (m, 2H, –OC**H**$_2$–), δ 3.50 (m, 2H, –C**H**$_2$N(C=O)CH$_2$CH$_2$CH$_2$), δ 3.39 (m, 2H, –N(C=O)CH$_2$CH$_2$C**H**$_2$), δ 2.33 (m, 2H, –N(C=O)CH$_2$C**H**$_2$CH$_2$), δ 1.90 (m, 2H, –N(C=O)C**H**$_2$CH$_2$CH$_2$) and δ 1.80 (d, 3H, C**H**$_3$C(=CH$_2$)–), as shown in Fig. S1.† Prior to use, the NMEP monomers were distilled at 140 °C under reduced pressure.

2.3 Synthesis of a PMMA or PDMAEMA macro-CTA

PDMAEMA and PMMA served as macro-CTAs for subsequent chain extensions. Both DMAEMA and MMA are commercially available monomers. Their purification involved: (i) passing through basic alumina to remove inhibitors and impurities; (ii) adding DPPH tprevent unintended polymerisation; (iii) introducing CaH_2 to eliminate moisture; and (iv) performing vacuum distillation on the day of polymerisation to ensure the purity of the monomers.

The detailed synthetic procedure for the macro-CTA is outlined below, using PMMA as an example. MMA monomer (12 g, 0.120 mol) was added to a 100 mL round-bottom Schlenk flask, along with the following components: CPDB (CTA, 1.06 g, 4.79 mmol; target DP = 25), AIBN (78.73 mg, 0.48 mmol; [CPDB] : [AIBN] = 10 : 1), and DMF (20.0 g). The Schlenk flask underwent freeze–pump–thaw cycles for 45 minutes and was then placed in a preheated oil bath at 70 °C for 12 hours. One portion of the PMMA sample was extracted for SEC and ^{1}H NMR analysis. Using ^{1}H NMR spectroscopy, the degree of polymerisation (DP) of the resulting macro-CTA was calculated, as shown in Fig. S2and S3.† Two peaks were selected for calculating DP: specifically, PMMA exhibited a signal at δ = 3.6 ppm attributed to the methyl protons at the end of its side chain, and a signal at δ = 7.8–8.0 ppm due to the aromatic protons on the end group of the RAFT agent.

2.4 Synthesis of PNMEP-based terpolymers and their diblock precursors

Following the successful synthesis of **PMMA** and **PDMAEMA** macro-CTAs, four amphiphilic terpolymers with different block orders (*i.e.* ABC, BAC, BCA and statistical) were prepared by sequential RAFT polymerisations on PMMA or PDMAEMA precursors, as depicted in Fig. 1.

The detailed synthetic route for MMA$_{22}$-*b*-DMAEMA$_{31}$-*b*-NMEP$_{18}$ (C2) serves as an illustrative example as follows: PMMA$_{22}$, used as the macro-CTA (2.27 g, 0.908 mmol), was combined in a 50 mL Schlenk flask with the DMAEMA monomer (5.0 g, 31.8 mmol), AIBN (22.4 mg, 0.136 mmol; [macro-CTA] : [AIBN] = 6.7 : 1), and DMF(6.75 g). After undergoing freeze–pump–thaw cycles, the reaction mixture was sealed, with the deoxygenated solution later heated in a preheated oil bath at 70 °C for 24 hours. The resulting diblock was then characterised using ^{1}H NMR and SEC to determine its structure and MM. The identified structure, MMA$_{22}$-*b*-DMAEMA$_{31}$, was precipitated in diethyl ether and served as the macro-CTA for the subsequent step.

The diblock macro-CTA (5.01 g, 0.66 mmol), NMEP monomer (2.6 g, 13.18 mmol), and AIBN (16.2 mg, 0.10 mmol; [macro-CTA] : [AIBN] ratio = 6.6 : 1) were dissolved in 1,4-dioxane (6.9 g) within a 50 mL Schlenk flask, and the mixture was deoxygenated using freeze–thaw cycles. Following a 24-hour reaction in a 70 °C-oil bath, the final product was obtained through precipitation in *n*-hexane. The ^{1}H NMR spectra of the final polymers and the precursors are presented in Fig. S4.† The statistical terpolymer (C4) was synthesised similarly to the triblock ones, with all comonomers, the CTA, and the free radical initiator added together at the beginning, yielding the final product in a single reaction step under identical conditions. The detailed reaction ratios for the RAFT polymerisations of all the terpolymers are listed in Table S1.†

2.5 Polymer characterisations

2.5.1 Size exclusion chromatography (SEC) measurements. The assessment of MM and dispersity was performed using an Agilent PL GPC-50 Integrated GPC/SEC System, which features a refractive index (RI) detector. The mobile phase consisted of HPLC-grade DMF with a concentration of 0.075% w/w lithium bromide (LiBr) and was maintained at a flow rate of 1.0 mL min^{-1} at a constant temperature of 40 °C. Sequential analysis was facilitated by the utilisation of two in-line GRAM Linear columns. The calibration protocol involved a set of PMMA standards with a low dispersity index. Polymer solutions were prepared by dissolving samples in HPLC-grade DMF containing 0.075% w/w LiBr to achieve a concentration of about 10 mg mL^{-1}. These solutions were then subjected to filtration using 0.45 μm PTFE filters prior to chromatographic evaluation. Calibration of the SEC was based on 12 PMMA standards with MMs of 0.54, 1.09, 1.81, 7.20, 13.90, 30.78, 72.80, 146.50, 260.90, 538.50, 1020.00, and 2210.00 kg mol^{-1}.

The theoretical MM for polymer synthesis could be calculated by employing the equation:

$$\mathrm{MM_{theo}}\,(\mathrm{g\,mol^{-1}}) = \sum_i \mathrm{MM}_i \times \mathrm{DP}_i + 221.34.$$

In this equation, the targeted DP of each block is multiplied by the MM of each comonomer and then added to the MM of the chain transfer agent CPDB.

2.5.2 Nuclear magnetic resonance (NMR) spectroscopy. For ^{1}H NMR, polymers were dissolved in $CDCl_3$ at a concentration

Open Access Article. Published on 07 June 2024. Downloaded on 6/20/2025 10:30:49 AM.
This article is licensed under a Creative Commons Attribution 3.0 Unported Licence.

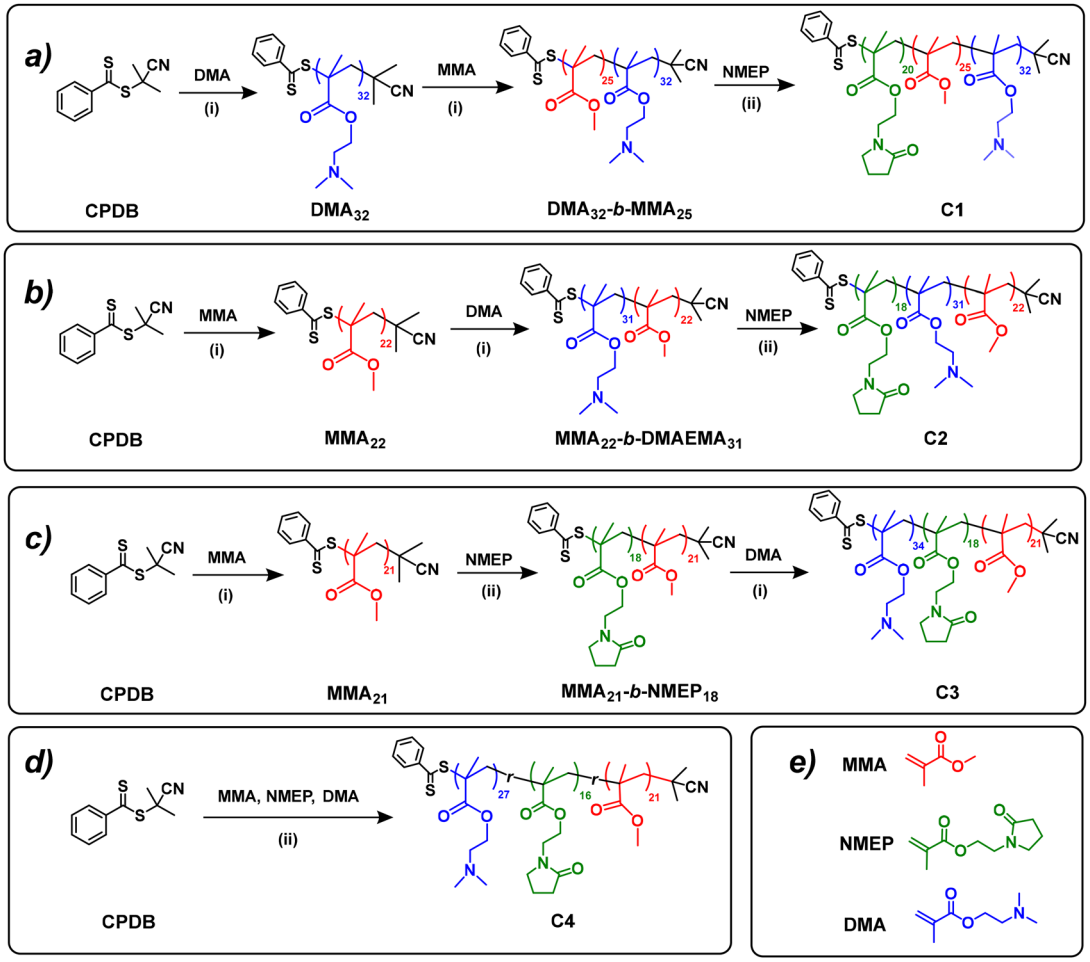

Fig. 1 Synthetic route of all amphiphilic terpolymers (C1–C4) in this study *via* RAFT polymerisation. Roman numerals (i) and (ii) indicate the reaction conditions: (i) reaction temperature of 70 °C with AIBN as the initiator and anhydrous DMF as the solvent, (ii) reaction temperature of 70 °C with AIBN as the initiator and 1,4-dioxane as the solvent.

of 10 mg mL^{-1} and analysed using a Jeol 400 MHz spectrometer. The experimental composition and the DP for each block were determined through ^{1}H NMR, with distinctive peaks assigned to each component: (i) for PMMA, the distinctive peak appears with proton resonance signals at δ = 3.55–3.60 ppm ((C═O)OC**H**$_3$), (ii) for PNMEP, the distinctive peak is observed with proton resonance signals at around δ = 2.00–2.13 ppm (–N(C═O)CH$_2$C**H**$_2$CH$_2$), (iii) for PDMAEMA, the distinctive peak is seen at around δ = 2.53–2.70 ppm ((C═O)OCH$_2$C**H**$_2$).

The temperature-dependent ^{1}H NMR analysis was also performed on the same machine for polymers dissolved in D$_2$O at a concentration of 10 mg mL^{-1}. Measurements were conducted at five different temperatures for each sample, including 25 °C, 30 °C, 35 °C, 40 °C, and 45 °C. The samples were allowed to settle at each temperature for 5 minutes prior to each measurement.

2.5.3 Turbidity measurements. 1% w/w polymer solutions in DI water were investigated by turbidity measurements, using a Cary UV-vis Compact Peltier Spectrometer (manufactured by Agilent, UK). The T_{cp}s were determined as the temperature at which the sample's transmittance dropped to 50%, with an instrumental error margin of ±1 °C for the T_{cp} measurements. The samples were heated at a rate of 1 °C per minute and held for 30 seconds between each measurement. Data collection occurred every 1 °C at a wavelength of 550 nm. The pH of the solutions was measured using a HI98103 pH checker, manufactured by Hanna Instruments, before measuring their respective T_{cp}. The T_{cp} of the polymers, under 10% protonation, was also measured after adding a calculated amount of 1M HCl to 1% w/w polymer solutions. The calculations for the amount of HCl added can be found in the ESI,† section 11.

2.5.4 Potentiometric titrations. 1% w/w aqueous polymer solutions were examined *via* hydrogen ion titrations. A HI98103 pH checker, manufactured by Hanna Instruments, was used to measure pH levels. The initial pH of polymer solutions, containing pH-responsive units of both NMEP and DMAEMA, were adjusted to 2 with 1 M HCl, and then 0.25 M NaOH was added stepwise to the resulting solution. The

Open Access Article. Published on 07 June 2024. Downloaded on 6/20/2025 10:30:49 AM. This article is licensed under a Creative Commons Attribution 3.0 Unported Licence.

effective pK_a of the terpolymers was determined to be the pH at which half of the ionisable groups were protonated. A titration curve for the terpolymers in this study was expected to reveal two equivalence points. The first and second pK_a values, corresponding to NMEP and DMAEMA respectively, were identified on the titration curve. pK_a1 was determined at the pH corresponding to half the volume at the first equivalence point, and pK_a2 was determined at the midpoint between the first and second equivalence points.

2.5.5 Dynamic light scattering (DLS) measurements. Aqueous polymer solutions (1% w/w) were analysed *via* DLS using a Zetasizer Nano ZSP. Before measurement, the solutions were filtered through PTFE filters with a 0.45 μm pore size to eliminate dust and large aggregates. DLS measurements of triblock terpolymers were conducted upon direct dissolution in DI water, while the statistical terpolymer was measured after 10% protonation. Each sample was assessed at ambient room temperature (25 °C) and during a temperature ramp test that spanned a range around its T_{cp}. At each temperature increment, the samples were allowed to settle for 120 seconds before measurements were taken. DLS measurements on the triblock terpolymer solutions, with pH adjusted to proposed values ranging from pH 2.0 to 10.0, were also conducted at 25 °C. The pH was adjusted by slowly adding 0.1 M NaOH or HCl, followed by measurement with a HI98103 pH checker, manufactured by Hanna Instruments.

The hydrodynamic diameters of triblock terpolymers, derived from the DLS, were subsequently compared to theoretically modelled values for a spherical micelle with fully extended chains. These values were based on the projected length of one methacrylate unit (0.254 nm) and the corresponding experimental DP. Specifically, the following equations were used: (i) for the ABC architecture, where the hydrophobic MMA is positioned as the middle block, the theoretical d_h is calculated as d_h (nm) = (DP_{MMA} + 2 × DP_{DMAEMA}) × 0.254 nm; (ii) for the BAC and BCA architectures, where the hydrophobic MMA forms a distinct block at the end of the polymer chain, the theoretical d_h is calculated as d_h (nm) = [DP_{MMA} + 2 × (DP_{DMAEMA} + DP_{NMEP})] × 0.254 nm; (iii) for the statistical terpolymer, the theoretical d_h is calculated as $\langle d_g^2 \rangle^{1/2} = 2 \times [2 \times 2.20 \times (DP_{NMEP} + DP_{DMAEMA} + DP_{MMA})/3]^{1/2} \times 0.154$ nm, assuming the formation of a random polymer coil.[50] The experimental DPs were calculated from their composition and MM values, which were determined previously *via* SEC and ^{1}H NMR analyses.

2.5.6 Transmission electron microscopy (TEM). TEM images were obtained with a JEOL STEM 2100 Plus Electron Microscope, under an operating voltage of 200 kV. All polymer solutions were prepared at a concentration of 1% w/w in DI water. Specifically, the statistical terpolymer (C4), while also prepared in DI water, required an additional step of 10% protonation to ensure solubility. Subsequently, approximately 10 μL of polymer solutions for each polymer sample were then pipetted onto a carbon film coated copper TEM grid from Agar Scientific. Excess polymer solution was carefully blotted with filter paper, and the sample was then negatively stained using around 20 μL of 2% w/v uranyl acetate for 1 minute.

2.5.7 Visual tests. The polymer solutions were visually examined using an IKA RCT heating hotplate and a continuously stirring water bath equipped with an IKA ETS-D5 temperature controller. The temperature was set to increase from 20 °C to 80 °C at a rate of 1 °C min^{-1}. Both the 1% w/w concentrated solutions (prepared in both DI water and PBS) and higher concentrated solutions, including 2%, 5%, 10%, 15%, and 20% w/w (prepared in PBS, pH 7.4 at 25 °C), were assessed for their thermal transitions. These assessments focused specifically on the light transmittance ability and resistance to flowing of the polymer solutions when the container was inverted. A stable thermogel was confirmed by conducting a simple but commonly employed "tube inversion" method across the temperature range, where the polymer solution does not flow when the vial is inverted.[51–53] The full thermal transitions were classified as follows, aligning with our previous studies:[46,54,55] (i) runny flowing solution (transparent, slightly cloudy, and cloudy); (ii) viscous solution (transparent and cloudy); (iii) stable gels (transparent and cloudy), where the sample does not flow when the vial is inverted; (iv) two phases: gel syneresis (disturbance in the gel due to internal stress) and precipitation (complete separation of the polymer solution into liquid and solid phases).

2.5.8 Rheological analysis. Rheology was performed on the polymer solutions in PBS using a TA Discovery HR-1 hybrid rheometer, equipped with a 40 mm-diameter Peltier steel plate. Polymer samples at a concentration of 20% w/w underwent oscillatory temperature ramp measurements to determine their changes in dynamic moduli, specifically the storage (G') and loss (G'') moduli, from 20 to 65 °C under a heating rate of 1 °C min^{-1}. The rheological gel and de-gel points, where relevant, were marked by the two crossovers between G' and G''.[56,57] In particular, the rheological gelation temperature (also called the gelation point), is the point at which G' exceeds G''. Sequentially, gel destabilisation may be observed at elevated temperatures where G' falls below G'', corresponding closely to either gel syneresis (T_{syn}) or gel precipitation (T_{prec}) noted during visual assessments.[58] Throughout these experiments, the angular frequency (ω) was set at 1 rad s^{-1} and the shear strain (γ) was maintained at 1%.

3. Results and discussion

3.1 Synthesis and characterisation of the terpolymers: molar mass, composition and pK_a

This research synthesised a series of PNMEP-based terpolymers through RAFT polymerisation, a method well-established in existing studies. Notably, prior works have utilised RAFT solution, dispersion, and emulsion polymerisation techniques,[40] which can be activated by either visible light[37,38] or temperature.[39,40] In this investigation, four unique PNMEP-based terpolymer structures – ABC, BAC, BCA, and statistical – were developed. The RAFT polymerisation process, employing

 This journal is © The Royal Society of Chemistry 2024

Open Access Article. Published on 07 June 2024. Downloaded on 6/20/2025 10:30:49 AM. This article is licensed under a Creative Commons Attribution 3.0 Unported Licence.

CPDB as the CTA and AIBN as the initiator, was conducted under conditions of 70 °C for durations of either 12 or 24 hours, as detailed in Table S1.†

The terpolymers in this study were synthesised from three distinct comonomers: A (DMAEMA), B (MMA), and C (NMEP). Comonomers A and C (DMAEMA and NMEP) are noted for their thermoresponsive properties, while B (MMA) imparts hydrophobic characteristics to the polymer. The synthesis targeted a consistent MM of 12 171 g mol^{-1}, with compositions across all architectures aiming for a specific ratio of 46% w/w DMAEMA, 21% w/w MMA, and 33% w/w NMEP. This ratio was selected based on preliminary findings that indicated the terpolymer's thermoresponsive behaviour is compromised, rendering it insoluble in deionised water when the MMA content exceeds 25% w/w. Specifically, a triblock copolymer of MMA-*b*-DMAEMA-*b*-NMEP was fabricated with a targeted 25% w/w MMA, which was found to be insoluble in water. Table 1 presents detailed structural information of these polymers, demonstrating compositions that closely align with the targeted values, within an acceptable deviation range. Further details, including SEC traces and ^{1}H NMR spectra with peak assignments and DP calculations, are provided in the ESI,† section 5–6.

In addition to their thermoresponsive nature, all synthesised polymers C1–C4 exhibit pH-responsiveness due to the tertiary amines present in both NMEP and DMAEMA components. Their pK_a values were determined through potentiometric titrations on 1% w/w aqueous polymer solutions. It is anticipated that the terpolymer components would display two distinct pK_a values corresponding to NMEP (~5.4) and DMAEMA (~7.5) respectively. The titration curve for the triblock terpolymer C1, along with the measured pK_a, is detailed in Fig. S6.† Similarly, the half-equivalent points of acid dissociation for C2–C4 were determined, with the findings summarised in Table 1. The measurements reveal that the pK_a values of the terpolymers, despite their varying architectures, are broadly consistent, with any deviations falling within the method's error margin. The pK_a of the statistical architecture was slightly lower, a result that aligns with findings from previous studies.[54,55]

3.2 Cloud point temperature (T_{cp}) measurements

Chemically, the NMEP units exhibit thermoresponsive properties arising from the combined effects of the pendant pyrrolidone groups and the apolar methacrylate backbone. Similarly, the thermoresponsive ability of DMAEMA units is attributed to the tertiary amine group on the side chain and the methacrylate backbone. However, DMAEMA's side chain is less polar than that of NMEP, leading to reduced solubility and a lower LCST in polymers with similar MM. This difference between NMEP and DMAEMA has been validated through research by Sun *et al.*,[59] Cunningham *et al.*,[39] and Billingham's group.[60]

Building upon the understanding of NMEP and DMAEMA, this study determined the T_{cp}s of NMEP-containing triblock terpolymers in DI water. Initially, a 1% w/w polymer solution was prepared, and the initial pH was recorded following its complete dissolution—a crucial step for accurate T_{cp} determination. This helps mitigate errors arising from pH variation or ionic impurities, enabling comparisons of T_{cp}s under different pH conditions and ensuring the precision of measurements. Notably, polymers C1, C2, and C3 exhibited initial pH values of 8.4, 8.0, and 8.7, respectively. Despite being dissolved in the same solvent and sharing similar polymer compositions, these polymers showed varying pH levels, likely due to their distinct architectures, which could influence the T_{cp}.

Upon 10% protonation, none of the block terpolymers exhibited a T_{cp} due to the increased hydrophilicity of the polymers. Protonation leads to the polymer micelles becoming positively charged at the tertiary amine groups in the NMEP and DMAEMA side chains, which in turn induces electrostatic repulsion between adjacent micelles. Such repulsion prompts the micelles to swell and maintain colloidal stability in water, a phenomenon extensively documented in previous

Table 1 Experimental polymer structure, targeted molar mass (MM_{target}) *versus* actual molar mass (M_n, determined by SEC), dispersity indices ($Đ$), compositions, and effective pK_a values of final polymers and their precursors (if applicable)

No.	Experimental polymer structure[a,b]	$MM_{(Target)}$ (g mol^{-1})	$M_{n\ (SEC)}$ [c] (g mol^{-1})	$Đ$	Composition[d] (% w/w)	pK_a [e]
C1	DMA_{32}	5724	4400	1.19	100–0–0	NA
	DMA_{32}-*b*-MMA_{25}	8227	7000	1.20	67–33–0	NA
	DMA_{32}-*b*-MMA_{25}-*b*-$NMEP_{20}$	**12 171**	**11 700**	1.28	44–22–34	5.4/7.5
C2	MMA_{22}	2724	2600	1.19	100–0–0	NA
	MMA_{22}-*b*-DMA_{31}	8227	7600	1.19	31–69–0	NA
	MMA_{22}-*b*-DMA_{31}-*b*-$NMEP_{18}$	**12 171**	**10 800**	1.30	21–46–33	5.4/7.6
C3	MMA_{21}	2724	2600	1.19	100–0–0	NA
	MMA_{21}-*b*-$NMEP_{18}$	6669	5200	1.25	37–63–0	NA
	MMA_{21}-*b*-$NMEP_{18}$-*b*-DMA_{34}	**12 171**	**11 200**	1.24	19–32–49	5.3/7.5
C4	MMA_{21}-*co*-$NMEP_{16}$-*co*-DMA_{27}	**12 171**	**9900**	1.18	24–29–47	5.2/7.4

[a] Abbreviations: NMEP, DMA, and MMA correspond to *N*-(2-(methacryloyloxy)ethyl) pyrrolidone, 2-(dimethylamino)ethyl methacrylate, and methyl methacrylate, respectively. Note that DMA is a further abbreviation of DMAEMA. [b] The experimental degrees of polymerisation (DP) of the polymers, after precipitation, were calculated using the M_n and the experimental compositions obtained by SEC and ^{1}H NMR analysis, respectively. [c] The number average molar mass (M_n) of the polymers was determined through SEC analysis after precipitation. [d] The composition of each component within the terpolymer in % w/w was calculated through ^{1}H NMR analysis. [e] The pK_a values of the final terpolymer products were determined by potentiometric titrations.

Open Access Article. Published on 07 June 2024. Downloaded on 6/20/2025 10:30:49 AM.
This article is licensed under a Creative Commons Attribution 3.0 Unported Licence.

Table 2 Cloud point temperature (T_{cp}) measurements for polymers C1–C4 in H_2O and D_2O at 1% w/w concentration

No.	Experimental polymer structure[a]	Architecture	Cloud point temperature, T_{cp}[b] (°C)		
			0% H^+ in H_2O	10% H^+ in H_2O	0% H^+ in D_2O
C1	DMA_{32}-*b*-MMA_{25}-*b*-$NMEP_{20}$	ABC	45	No T_{cp}	37
C2	MMA_{22}-*b*-DMA_{31}-*b*-$NMEP_{18}$	BAC	45	No T_{cp}	36
C3	MMA_{21}-*b*-$NMEP_{18}$-*b*-DMA_{34}	BCA	35	No T_{cp}	29
C4	MMA_{21}-*co*-$NMEP_{16}$-*co*-DMA_{27}	Statistical	NS[c]	25	NS[c]

[a] Abbreviations: 2-(dimethylamino)ethyl methacrylate (DMA), methyl methacrylate (MMA), *N*-(2-(methacryloyloxy)ethyl) pyrrolidone (NMEP). Note that DMA is a further abbreviation of DMAEMA. [b] The cloud point temperature (T_{cp}) was determined by turbidimetry. [c] The determination of T_{cp} for the statistical terpolymer was not feasible as it is insoluble at 0% protonation.

studies.[61–65] However, the statistical terpolymer C4 was an exception; it only became soluble after 10% protonation, which makes the polymer more hydrophilic, thus enabling the measurement of its T_{cp} at 25 °C, as detailed in Table 2. The reduced solubility of the statistical terpolymer compared to their block-based counterparts, due to its inability to form micelles, is well documented in previous studies.[54,55,66]

3.3 Temperature variation ^{1}H NMR

3.3.1 Solvent isotopic effect on thermoresponsive behaviours. The T_{cp}s of the triblock terpolymers C1–C3 in deuterium oxide (D_2O) were also determined with turbidimetry. It was observed that all triblock terpolymers exhibited a T_{cp} that was systematically 6–9 °C lower in D_2O than in H_2O, regardless of their architectures, as depicted in Fig. 2. This phenomenon aligns with findings reported by Liu *et al.*[67] and Sun *et al.*,[59] who investigated similar behaviours in other polymers, particularly those containing pyrrolidone functional groups.

Sun *et al.* attributed the lower T_{cp} in D_2O to the absence of hydrogen bonding donors in PNMEP, coupled with weaker van der Waals interactions such as hydrophobic associations of apolar backbones and spacers.[59] Extending this concept to our study, which also involves comonomers NMEP and DMAEMA —similar to NMEP—lacking hydrogen bonding donors on their side chains, suggests that the interactions of such polymers with D_2O inherently lack hydrogen bonding and result in a lower T_{cp}. This phenomenon has also been reported by Cremer's group in elastin-like peptides (ELPs),[68] which exhibit a more stabilised collapsed state in D_2O than in H_2O, thus displaying a lower T_{cp}.

However, this mode of interaction stands in contrast to that observed in polymers like PNIPAM, which exhibit a higher T_{cp} in D_2O compared to H_2O. This is likely attributed to PNIPAM's stronger hydrogen bonding with D_2O molecules, resulting in higher bond strength and an increased enthalpic cost to break these hydrogen bonds.[69–71] This difference is possibly due to the fact that NIPAM units have a secondary amine with a hydrogen next to the nitrogen, free to form hydrogen bonds, while both NMEP and DMAEMA units have a tertiary amine with no free hydrogen to form hydrogen bonds.

3.3.2 Temperature variation ^{1}H NMR on the thermoresponsive behaviours. The thermal behaviour of terpolymers C1, C2, and C3 was carefully characterised using ^{1}H NMR spectroscopy in D_2O at a concentration of 10 mg mL^{-1}. Measurements were conducted over a temperature range from 25 to 45 °C, in increments of 5 °C. This range was chosen based on the T_{cp} observed in D_2O, which were anticipated to be 37 °C, 36 °C, and 29 °C for C1, C2, and C3, respectively.

Fig. 3 reveals that at 25 °C, all three terpolymers display clear and detectable proton resonance signals in D_2O, confirming their good solubility at room temperature and near their respective T_{cp}. Notably, a significant decrease in these proton

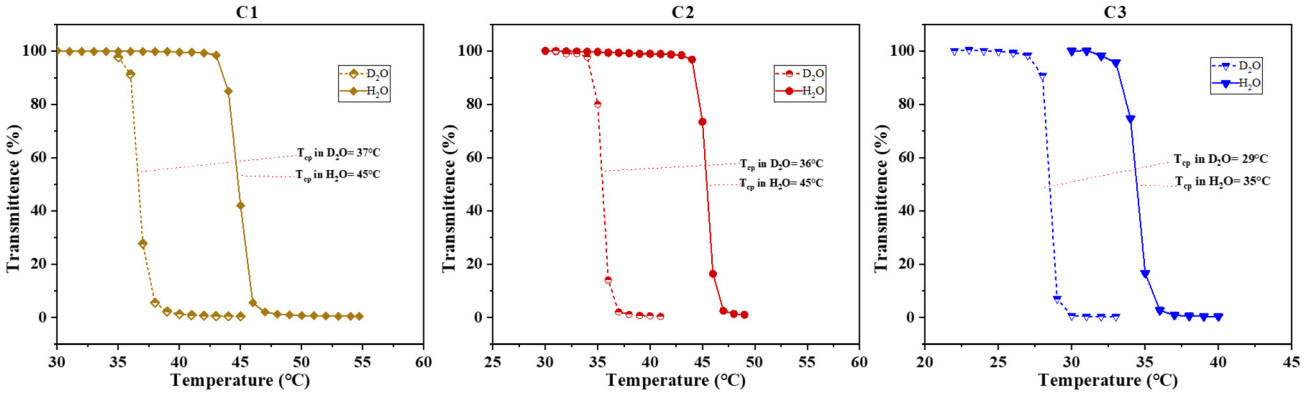

Fig. 2 Transmittance plotted as a function of solution temperature for the T_{cp} determination of polymers C1, C2 and C3 (from left to right) in both D_2O and H_2O.

 This journal is © The Royal Society of Chemistry 2024

Open Access Article. Published on 07 June 2024. Downloaded on 6/20/2025 10:30:49 AM.
This article is licensed under a Creative Commons Attribution 3.0 Unported Licence.

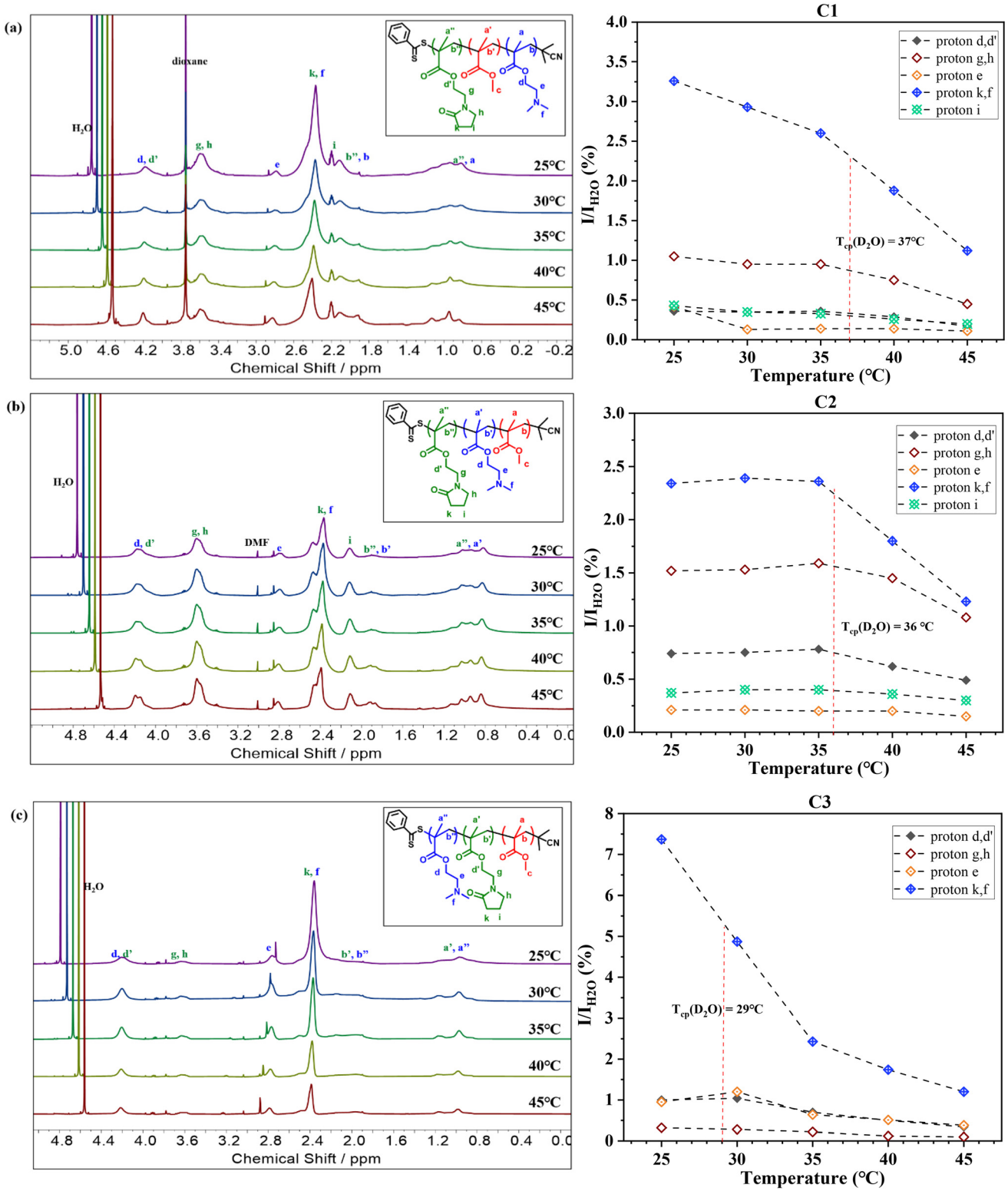

Fig. 3 Temperature-variation ^{1}H NMR spectra and corresponding proton integration ratios for a 10.0 mg mL^{-1} sample of (a) C1, DMA$_{32}$-*b*-MMA$_{25}$-*b*-NMEP$_{20}$ (b) C2, MMA$_{22}$-*b*-DMA$_{31}$-*b*-NMEP$_{18}$ and (c) C3, MMA$_{21}$-*b*-NMEP$_{18}$-*b*-DMA$_{34}$ in D_2O to that of H_2O (I/I_{H_2O}), plotted as a function of solution temperature.

Open Access Article. Published on 07 June 2024. Downloaded on 6/20/2025 10:30:49 AM. This article is licensed under a Creative Commons Attribution 3.0 Unported Licence.

resonance signals was observed upon reaching their T_{cp} in D_2O, suggesting reduced chain mobility at elevated temperatures.

Further analysis involved calculating the relative integral ratios of protons from NMEP and DMAEMA to the integral of H_2O in each terpolymer, as illustrated in Fig. 3. This analysis validated the reduction in proton integrals for all three terpolymers above the T_{cp}. It was observed that the sharpest drop in proton integrals occurs in the peak with a chemical shift around 2.25–2.65 ppm. This drop is attributed to both the protons in the pyrrolidone ring of NMEP (2H, $NCOC\mathbf{H}_2CH_2CH_2$, δ = 2.45 ppm) and the protons of methyl groups in the tertiary amine of DMAEMA (6H, $-N(C\mathbf{H}_3)_2$, δ = 2.35 ppm).

While most proton resonance signals identifiable in $CDCl_3$ were also detectable in D_2O, C3 (MMA_{21}-*b*-$NMEP_{18}$-*b*-$DMAEMA_{34}$) was an exception. As shown in Fig. 3(c), this terpolymer exhibited markedly weak signals for NMEP protons, particularly protons g and h, and a complete absence of proton i, in contrast to the other terpolymers. Notably, in C3, the only clearly detectable NMEP proton peaks—d and d′, k and f, a′ and a″, b′ and b″—are attributed simultaneously to both NMEP and DMAEMA. This suggests that the detectability of these peaks may be primarily due to DMAEMA's influence, rather than NMEP's.

This observation highlights the distinct molecular architecture of C3, which forms a core–shell-corona structure with a permanently hydrophobic MMA core, a partially desolvated NMEP inner shell, and a thick and well-solvated DMAEMA corona. Consequently, NMEP exhibits a hydrophobic character and collapses onto the MMA hydrophobic core when positioned as the middle block. This type of core–shell-corona micelle structure, featuring a pH- or thermo-responsive shell to promote pH- or temperature-induced micellization, has been studied under ^{1}H NMR analysis in D_2O and is well-documented in the literature.[72–75]

This architectural influence also sheds light on the unconventional T_{cp} trends observed in these triblock terpolymers. Notably, C1 and C2, despite having different architectures, exhibit surprisingly similar T_{cp} values. In contrast, C2 and C3, both incorporating hydrophobic MMA as their outer block, demonstrate distinctly different T_{cp} values. This variation can be attributed to the terpolymers' differing degrees of hydration/solvation of the blocks, influenced by their structural differences, as evidenced by the change in intensity of the signals for different terpolymer architectures under ^{1}H NMR analysis in D_2O. Specifically, in C3, the positioning of NMEP as the middle block contributes to its more solvophobic properties, resulting in much attenuated signals under ^{1}H NMR, which in turn affects its thermoresponsive ability. Consequently, the T_{cp} of C3 is predominantly influenced by the thermoresponsive behaviour of DMAEMA at the outer corona, unlike in C1 and C2, where it is affected by the mutual impact of both NMEP and DMAEMA blocks, resulting in a lower T_{cp} compared to C1 and C2.

3.4 Self-assembly behaviour

3.4.1 Particle size and configurations of the terpolymers. DLS was used to study the self-assembly behaviour of the polymers. As mentioned above, except for C4, the insoluble statistical terpolymer, all triblock terpolymers were water-soluble. In Table 3, the theoretical diameters and the experimentally determined diameters of all polymers are presented. The results indicated that the triblock terpolymers can self-assemble into micelles with diameters ranging from 15 to 35 nm. Theoretical calculations, based on our proposed model that accounts for the formation of fully extended spherical micelles in an aqueous medium (as shown in Table 3), suggest that the diameter should decrease from polymer C3 (BCA) to C2 (BAC), with C1 (ABC) having the smallest diameter. These theoretical values were based on the projected length of one methacrylate unit (0.254 nm) and the corresponding experimental DP. Specifically, the following equations were used: (i) for the ABC architecture, where the hydrophobic MMA is positioned as the middle block, the theoretical d_h is calculated as d_h (nm) =

Table 3 Hydrodynamic diameter measured by DLS for C1–C4

No.	Experimental polymer structure[a]	Architecture	Hydrodynamic diameter (±0.5 nm)		
			Theoretical[b]	By intensity	By number
C1	DMA_{32}-*b*-MMA_{25}-*b*-$NMEP_{20}$	ABC	22.6	15.7	6.3
C2	MMA_{22}-*b*-DMA_{31}-*b*-$NMEP_{18}$	BAC	30.5	27.4	11.7
C3	MMA_{21}-*b*-$NMEP_{18}$-*b*-DMA_{34}	BCA	31.8	18.2	7.5
C4	MMA_{21}-*co*-$NMEP_{16}$-*co*-DMA_{27}	Statistical	3.0	4.2[c]	2.3[c]

[a] Abbreviations: 2-(dimethylamino)ethyl methacrylate (DMA), methyl methacrylate (MMA), *N*-(2-(methacryloyloxy)ethyl) pyrrolidone (NMEP). Note that DMA is a further abbreviation of DMAEMA. [b] The theoretical hydrodynamic diameter was calculated by assuming the formation of either a classical core–shell micelle or a polymer coil. Specifically, the following equations were used: (i) for the ABC architecture, where the hydrophobic MMA is positioned as the middle block, the theoretical d_h is calculated as d_h (nm) = $(DP_{MMA} + 2 \times DP_{DMAEMA}) \times 0.254$ nm; (ii) for the BAC and BCA architectures, where the hydrophobic MMA forms a distinct block at the end of the polymer chain, the theoretical d_h is calculated as d_h (nm) = $[DP_{MMA} + 2 \times (DP_{DMAEMA} + DP_{NMEP})] \times 0.254$ nm; (iii) for the statistical terpolymer, the theoretical d_h is calculated as $\langle d_g^2 \rangle^{1/2} = 2 \times [2 \times 2.20 \times (DP_{NMEP} + DP_{DMAEMA} + DP_{MMA})/3]^{1/2} \times 0.154$ nm, assuming the formation of a random polymer coil. Here, the experimental degrees of polymerisation were used, calculated by multiplying the actual molar mass obtained from SEC with the actual composition determined by ^{1}H NMR. [c] The hydrodynamic diameter and T_{cp}s of the statistical terpolymer were measured under 10% H^+ protonation, as this polymer was insoluble in aqueous solutions without any protonation. Notably, the hydrodynamic diameter of the statistical terpolymer was measured at 10 °C, instead of room temperature (25 °C), due to its cloud point being close to room temperature, which could affect the measurement.

 This journal is © The Royal Society of Chemistry 2024

Open Access Article. Published on 07 June 2024. Downloaded on 6/20/2025 10:30:49 AM.
This article is licensed under a Creative Commons Attribution 3.0 Unported Licence.

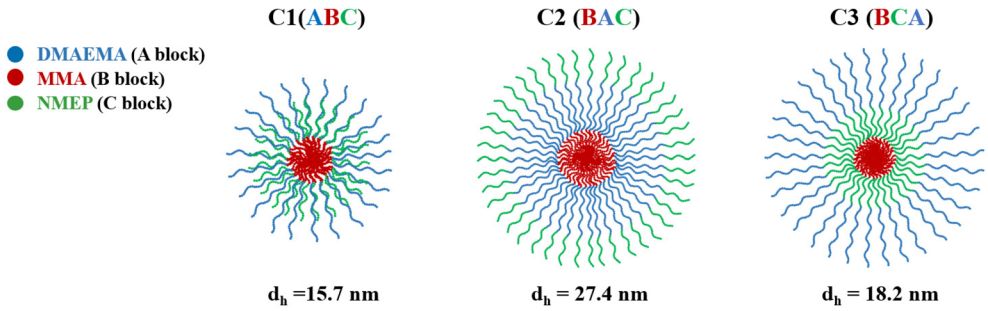

Fig. 4 Schematic representation of the proposed micelle configuration and the hydrodynamic diameters as measured by DLS for C1, C2, and C3.

(DP_{MMA} + 2 × DP_{DMAEMA}) × 0.254 nm; (ii) for the BAC and BCA architectures, where the hydrophobic MMA forms a distinct block at the end of the polymer chain, the theoretical d_h is calculated as d_h (nm) = [DP_{MMA} + 2 × (DP_{DMAEMA} + DP_{NMEP})] × 0.254 nm. The experimental DPs were calculated from their composition and MM values, which were determined *via* SEC and ^{1}H NMR analyses.

Therefore, the model predicts that C1, characterised by its ABC structure and a central hydrophobic block, forms smaller and structurally distinct micelles compared to C2 and C3, which have hydrophobic MMA at the end of their chains. As depicted in the configuration schematics in Fig. 4, C1 with the centrally located MMA likely contributes to a hydrophilic corona with a thickness comparable to DMAEMA. Conversely, C2 and C3, with terminal MMA, are expected to form micelles with thicker and more extended hydrophilic shells consisting of both DMAEMA and NMEP.

Empirical DLS data supports the theoretical predictions, with C1 showing the smallest diameter compared to the other two. Specifically, the DLS results indicate a descending size order of C2, C3, and C1, with C2 being approximately 1.5 to 2 times larger than the others. The measured micelle diameters are consistently smaller than the theoretically predicted values. This discrepancy between empirical and theoretical values was expected and has been previously reported,[54,55,66] attributed to the model assuming fully stretched polymer chains.

This size sequence is also consistent with our group's earlier studies on amphiphilic triblock terpolymer systems based on comonomers with slight variations, namely oligo (ethylene glycol) methyl methacrylate (OEGMA, average M_n = 232.27 or 300 g mol^{-1}).[55,66] Similar to our current findings, those studies reported a size sequence of BAC, BCA, and ABC, with 'A' denoting DMAEMA, 'B' denoting butyl methacrylate, and 'C' denoting OEGMA instead of NMEP.

Meanwhile, the size of the statistical polymer was measured by DLS at 10% protonation, since it is insoluble at 0% protonation. The theoretical d_h for the statistical terpolymer is calculated as $\langle d_g^2\rangle^{1/2}$ = 2 × [2 × 2.20 × (DP_{NMEP} + DP_{DMAEMA} + DP_{MMA})/3]$^{1/2}$ × 0.154 nm, assuming the formation of a random polymer coil.[50] The experimental hydrodynamic diameter was measured to be 4.2 nm, which is close to the theoretically predicted value, and also aligns with our expectation that this polymer cannot self-assemble into micelles but mainly exists as coils.

3.4.2 Particle size and pH dependence of the triblock terpolymers. The pH-responsiveness of this polymer, attributed to two amine-containing blocks, was monitored by DLS. Specifically, changes in the hydrodynamic diameters of their self-assemblies were observed across different pH levels from 10 to 2. It is noteworthy that the pH was adjusted in a singular direction from its original value, either towards a higher pH using diluted NaOH (0.1 M) or towards a lower pH using HCl (0.1 M). As depicted in Fig. 5(a), the *z*-average d_h of polymer micelles is seen to vary with pH, since the ionisation state of the amine groups within the polymers is influenced by the pH of the environment.

Fig. 5(c) demonstrates that upon increasing the pH from 8.0 to 10.0 through titration with OH^-, the *z*-average particle sizes remain largely unchanged, exhibiting only a slight decrease. This decrease is attributed to the deprotonation of the corona at pH levels exceeding the pK_a values of both pH-responsive blocks, resulting in more compact micelle structures and a consequent reduction in hydrodynamic diameter.

Conversely, titration of the polymer sample with H^+ to decrease the pH from 8.0 to 2.0 leads to protonation of the tertiary amine groups (R_3N) in both NMEP and DMAEMA comonomers, converting them to their positively charged forms (R_3NH^+). This protonation significantly impacts the overall morphology and size of the micelles. Specifically, as the pH decreases from 8.0 to 6.0, a gradual increase in particle size is observed due to the increased protonation, causing the polymer to transition from a hydrophobic to a hydrophilic state and resulting in the formation of swollen micellar structures.

Further titration of the polymer solution from pH 6.0 to pH 4.0 results in more pronounced changes in hydrodynamic diameter, indicating significant alterations in the ionisation state of the polymers. This effect is especially noticeable as the pH drops below 5.3, the pK_a of the PNMEP blocks. At these lower pH levels, the corona, which is pH-responsive, becomes increasingly hydrophilic, swollen, and loose, leading to a heightened tendency to form aggregates. As the pH continues to decrease to between 4.0 and 2.0, the terpolymers become

Open Access Article. Published on 07 June 2024. Downloaded on 6/20/2025 10:30:49 AM.
This article is licensed under a Creative Commons Attribution 3.0 Unported Licence.

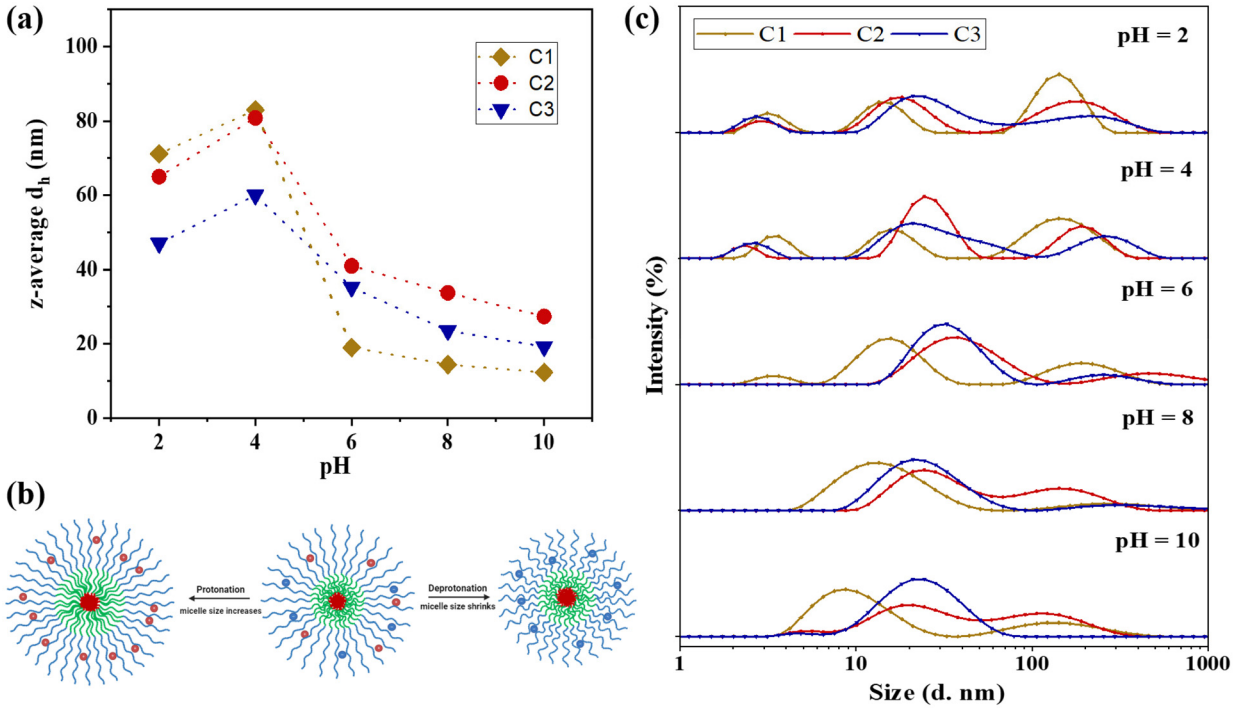

Fig. 5 (a) Changes in the z-average d_h against different pH values for C1, C2, and C3. (b) Schematic demonstrating the impact of protonation on the terpolymer (C3) and its sizes. (c) Particle size distribution by intensity under varying pH levels: 2, 4, 6, 8, and 10.

fully protonated, further enhancing their hydrophilicity. This leads to a reduction in aggregation number due to excessive protonation and electrostatic repulsions, as well as a slight dissociation of the micelles into unimer structures resulting from the dissolution of polymer chains, which contributes to a minor decrease in overall particle size. Furthermore, at this pH, there is also a higher ionic strength from adding more HCl, and the excess of Cl^- are counteracting the cationic charges of the tertiary amines, thus allowing the chains to be slightly less stretched. This charge screening has been previously reported in crosslinked amino-containing gels.[76] It should be noted that the change in hydrodynamic diameters within this low pH range is more pronounced for C1 and C2, compared to the less significant change for C3. This disparity can be attributed to the architectural effect: in C3, the NMEP block is located in the inner shell, sterically surrounded by the thick outer corona consisting of the DMAEMA block, which decreases the degree of hydration of NMEP, as previously discussed.

The above findings are in line with previous studies on the pH-responsive behaviour of PDMAEMA-containing polymers, which have similarly reported changes in particle sizes in response to varying pH levels.[77–79]

3.5 Transmission electron microscopy images

TEM images were taken for all terpolymer samples to visualize their configurations and compared with their DLS results. It is worth noting that TEM samples were prepared from polymer solutions in DI water without adjusting the pH for the triblock terpolymers. However, the sample was titrated to 10% protonation for the statistical terpolymer (C4) to ensure solubility. The TEM results confirm the formation of spherical-like micelles by the block terpolymers, as expected. In contrast, the statistical terpolymer does not exhibit a definitive shape of micelles in the TEM images. The diameter of these polymer particles was measured from TEM images with standard deviations calculated, and then compared with the hydrodynamic diameter, as shown in Fig. 6.

It is observed that both results align well with each other. Specifically, the diameter size increases from C1 to C3 to C2, consistent with observations from DLS. The diameters determined by TEM are smaller than the DLS values, as expected and observed in previous research.[46,55,80] This discrepancy is attributed to different sample conditions. Specifically, TEM analysis is performed on dried samples, where the absence of water leads to the collapse of hydrophobic and hydrophilic segments of the micelles, resulting in smaller measurements. In contrast, DLS is conducted in aqueous conditions, measuring the hydrodynamic radius that includes both the micelle and its hydration shell, yielding larger size estimations. Therefore, the 'drying effect' in TEM removes the water that normally hydrates and swells the micelle structures. Unlike DLS, which measures the hydrodynamic radius including the solvation layer of water molecules around the polymer particle, only the solid components of the micelles are visible in TEM, making them inherently smaller.[81]

Overall, TEM provides a visual representation of all particles in the field of view and confirms the spherical micelles formed

Open Access Article. Published on 07 June 2024. Downloaded on 6/20/2025 10:30:49 AM.
This article is licensed under a Creative Commons Attribution 3.0 Unported Licence.

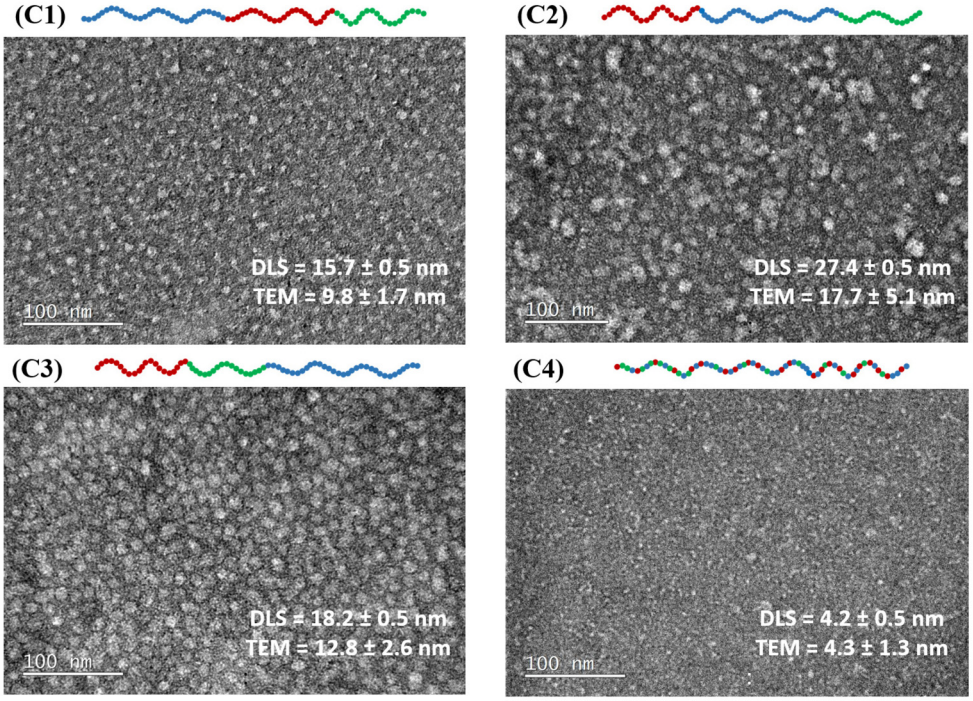

Fig. 6 TEM images were obtained with the samples negatively stained using 1% w/w uranyl acetate, showing C1 (ABC), C2 (BAC), C3 (BCA), and C4 (statistical) dissolved in DI water at 1% w/w. Note that C4 was prepared in a solution with 10% protonation to ensure solubility. Particle sizes in the TEM images were estimated using the measuring scales located in the left corner of each figure and were then compared with their hydrodynamic diameters measured by DLS.

by the triblock terpolymers, as well as the absence of self-assembled structures in the statistical terpolymer sample. By comparing the results measured by DLS and TEM, the differences in size and conformation of the terpolymers in various architectures were verified.

3.6 Visual test and rheology

3.6.1 Phase diagram construction *via* visual observation. The thermal transitions of triblock terpolymers were observed by conducting visual tests, as described in the experimental section, by heating the polymer solutions in PBS at 1 °C min^{-1} in a concentration range from 1% w/w up to 20% w/w. The statistical terpolymer was not investigated in this case due to its insolubility in PBS. At a lower concentration of 1% w/w, we found polymer samples displayed a similar trend as their T_{cp} in DI water, wherein the ABC architecture exhibited a higher T_{cp} compared to BAC or BCA. However, all T_{cp}s in PBS were at systematically lower temperatures than those detected for their polymer solutions in pure water, attributed to the ionic 'salting-out' effect.[82,83]

Polymer solutions with higher concentrations are more prone to thermogel formation due to their enhanced ability to entangle and create physical cross-links within a 3D network. To evaluate the polymer's gelation behaviour—the transition from a sol to a gel—a "tube inversion" test was conducted. This test determined whether the sample remained fluid upon inverting the vial. The gelation region, when present, was marked on the phase diagrams with a blue-coloured symbol, as illustrated in Fig. 7. Interestingly, two of the three polymers studied, C2 and C3, which possess BAC and BCA architectures with a hydrophobic end block instead of the ABC configuration, underwent thermal gelation transitions. This observation deviates from our previous studies on the architectural influence in different triblock terpolymer systems.[54,55,84] Those studies suggested that polymers with an ABC architecture typically displayed a more well-defined sol–gel transition, characterised by a wider gelation region, a lower critical gelation concentration, and the formation of a mechanically stronger gel. However, it is important to note that in those previous studies, only one monomer was ionic, which could significantly affect the thermoresponsive sol–gel transitions observed. Regarding this study, the structure of the triblock terpolymer, featuring two ionic end blocks, might influence the formation of micelle-bridging links essential for gelation.

3.6.2 Rheological characterisation. As stable gel formation was observed only in C2 and C3 in highly concentrated polymer solutions (over 15% w/w), this indicates that the minimum threshold for polymer entanglements was achieved in these systems. Consequently, for the rheological measurement of their dynamic moduli (G' and G'') during a temperature ramp, 20% w/w concentrated PBS-based polymer solutions were selected for all three terpolymers. This helps to provide mechanical insights into a polymer solution by measuring flow and deformation under shear stress. The

Open Access Article. Published on 07 June 2024. Downloaded on 6/20/2025 10:30:49 AM.
This article is licensed under a Creative Commons Attribution 3.0 Unported Licence.

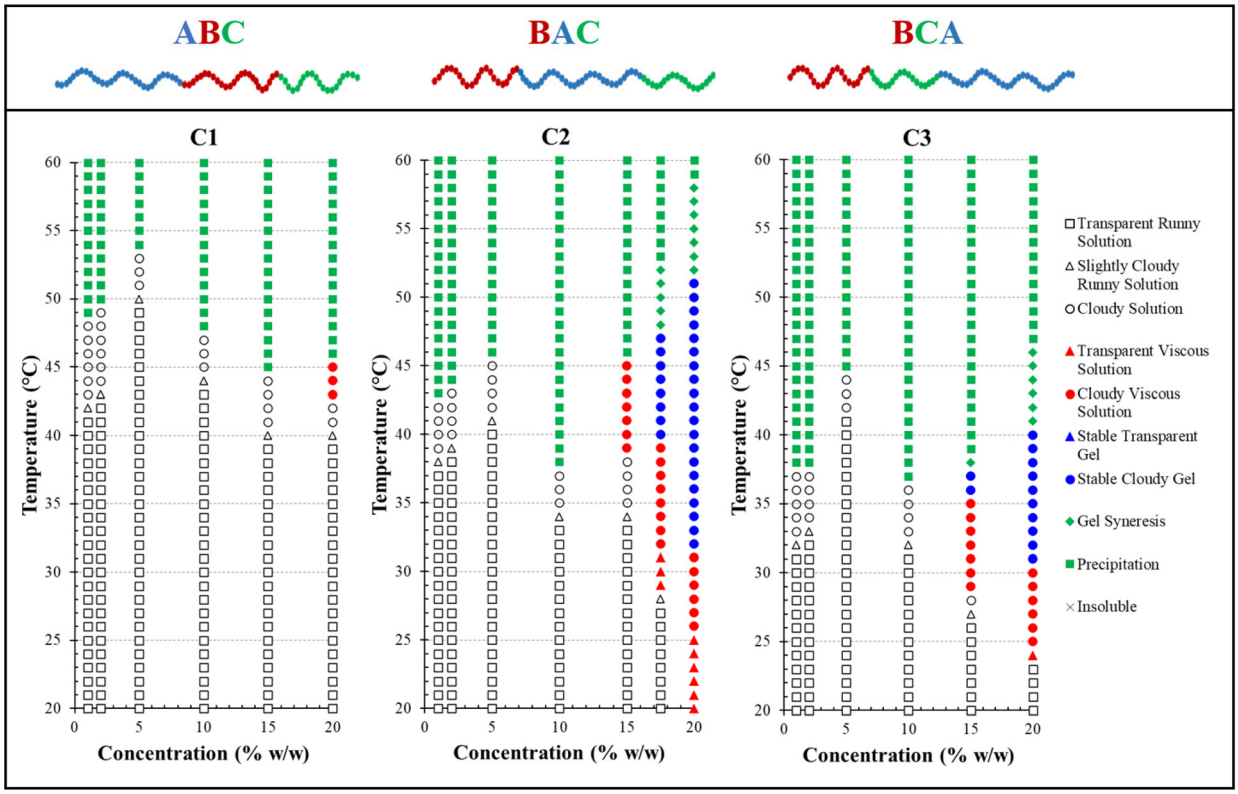

Fig. 7 Phase diagram of C1–C3, plotted using visual observation results for polymer solutions prepared in PBS (pH = 7.4) at concentrations of 1% w/w, 2% w/w, 5% w/w, 10% w/w, 15% w/w, and 20% w/w. Visual transition states are reported as: (a) runny solution in white, (b) viscous solution in red, (c) stable gel in blue, and (d) phase separation in green.

crossover between the storage and loss moduli ($G' > G''$) was identified as the gelation point, indicating the establishment of a three-dimensional polymer network capable of resisting deformation and providing mechanical support.[56,57] On the other hand, no crossover ($G'' < G'$) at any temperature of interest was observed for the polymer that did not exhibit thermo-responsive sol–gel transitions, *i.e.* C1.

The rheological behaviour of these polymers should correlate with their visual characteristics, particularly at critical transition points identified by both rheological measurements and visual inspections. The critical temperatures include the gelation temperature (T_{gel}) and degel temperature (T_{degel}) from rheological data, as well as the gelation temperature (T_{gel}), syneresis temperature (T_{syn}), and precipitation temperature (T_{prec}) from visual observations. In rheology, T_{gel} is the temperature at which G' exceeds G'', indicating the gel point, while T_{degel} is the temperature at which G'' exceeds G' again, showing that viscous flow is more significant than elastic deformation. For visual observations, T_{syn} marks the onset of gel syneresis (defined as disturbance in the gel due to internal stress),[85] and T_{prec} indicates the start of precipitation (the complete separation into solid and aqueous phases).

Table 4 demonstrates that rheological measurements are consistent with the visual test results. Specifically, these

Table 4 Theoretical chemical structure and critical temperatures, including gelation temperature (T_{gel}), syneresis temperature (T_{syn}), and precipitation temperature (T_{prec}) from visual tests, as well as gelation (T_{gel}) and degelation points (T_{degel}) examined by rheology

			Critical temperatures (°C)				
			Visual test (±2 °C)			Rheology (±1 °C)	
No.	Experimental chemical structure[a]	Architecture	T_{gel}	T_{syn}	T_{prec}	T_{gel}	T_{degel}
C1	DMA_{32}-*b*-MMA_{25}-*b*-$NMEP_{20}$	ABC	NA				
C2	MMA_{22}-*b*-DMA_{31}-*b*-$NMEP_{18}$	BAC	32	52	59	32	51
C3	MMA_{21}-*b*-$NMEP_{18}$-*b*-DMA_{34}	BCA	31	41	48	33	40

[a] Abbreviations: 2-(dimethylamino)ethyl methacrylate (DMA), methyl methacrylate (MMA), *N*-(2-(methacryloyloxy)ethyl) pyrrolidone (NMEP). Note that DMA is a further abbreviation of DMAEMA.

 This journal is © The Royal Society of Chemistry 2024

Open Access Article. Published on 07 June 2024. Downloaded on 6/20/2025 10:30:49 AM.
This article is licensed under a Creative Commons Attribution 3.0 Unported Licence.

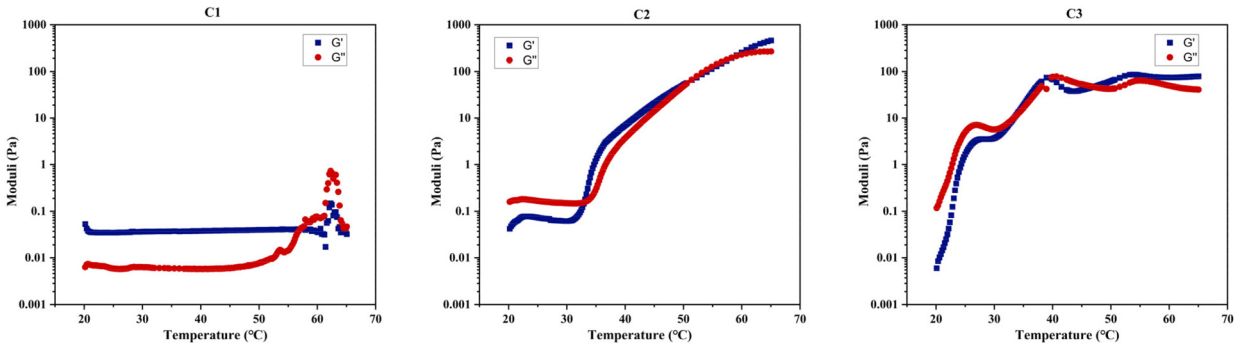

Fig. 8 Rheological measurements during a 1 °C min^{-1} temperature scan from 20 to 65 °C under a constant shear strain of 1% (γ) for C1–C3 dissolved in PBS at 20% w/w.

measurements confirm C1's lack of gelation, evidenced by the absence of a crossover or notable increase between its two dynamic moduli within the examined temperature range, as shown in Fig. 8. This behaviour suggests that C1 (ABC) predominantly exhibits viscous, liquid-like characteristics. In contrast, the gelation temperatures for C2 (BAC) and C3 (BCA), as determined by both testing methods, show a minor discrepancy of 1–2 °C, which is within the acceptable experimental error margin of the techniques.

A clear difference in gelation behaviour between C2 and C3 can be observed from both Table 4 and Fig. 8: C2 (BAC) has a gelation window spanning approximately 20 °C, while C3 (BCA) has a gelation window of approximately 10 °C. Additionally, C2 demonstrates a gradual increase in gel strength as the temperature rises, whereas C3 shows less variation in G′, upon examining their changes in the storage modulus with temperature for 20% w/w concentrated polymer solutions in PBS. The storage modulus is key to indicating the energy elastically stored within the gel during deformation, signifying a shift towards solid-like behaviour and a mechanically stronger network that can retain its shape when subjected to oscillatory shear deformation. Therefore, both C2 and C3 should be classified as 'weak gels',[86,87] based on the maximum G' values recorded for both polymers before reaching their degradation temperatures, consistently remaining below 100 Pa, despite C2 forming a stronger gel as temperature increases.

4. Conclusions

In this study, pyrrolidone-based amphiphilic thermoresponsive terpolymers were synthesised through reversible addition–fragmentation chain transfer (RAFT) polymerisation, examining four unique terpolymer architectures: ABC, BAC, BCA, and statistical. The molar masses and compositions were kept similar across the terpolymers to investigate the influence of polymer architecture on their self-assembly conformations and thermoresponsive characteristics by employing techniques such as Turbidimetry, Dynamic Light Scattering, Transmission Electron Microscopy, temperature-dependent ^{1}H NMR spectroscopy, and rheometry. Notably, the terpolymers exhibited a lower cloud point temperature in D_2O than in H_2O and showed enhanced hydrophilicity at 10% protonation. While all block terpolymers formed spherical micelles whose sizes were influenced by pH changes, the statistical terpolymer did not. The arrangement of the block architecture and the position of hydrophobic groups were found to significantly influence thermoresponsive behaviour, with the BAC and BCA architectures demonstrating a clear sol–gel transition. This research highlights the vital importance of the comonomer arrangement in pyrrolidone-based terpolymers, offering significant insights for their application in the development of stimuli-responsive materials.

Conflicts of interest

There are no conflicts to declare.

Acknowledgements

EPSRC is acknowledged for HI's funding (EP/W034093/1).

References

1 A. Bordat, T. Boissenot, J. Nicolas and N. Tsapis, *Adv. Drug Delivery Rev.*, 2019, **138**, 167–192.
2 D. Roy, W. L. A. Brooks and B. S. Sumerlin, *Chem. Soc. Rev.*, 2013, **42**, 7214–7243.
3 M. R. Matanović, J. Kristl and P. A. Grabnar, *Int. J. Pharm.*, 2014, **472**, 262–275.
4 W. Tao, J. Wang, W. J. Parak, O. C. Farokhzad and J. Shi, *ACS Nano*, 2019, **13**, 4876–4882.
5 X. Pang, Y. Jiang, Q. Xiao, A. W. Leung, H. Hua and C. Xu, *J. Controlled Release*, 2016, **222**, 116–129.
6 E. Pantuso, G. De Filpo and F. P. Nicoletta, *Adv. Opt. Mater.*, 2019, **7**, 1900252.
7 B. Sana, A. Finne-Wistrand and D. Pappalardo, *Mater. Today Chem.*, 2022, **25**, 100963.

Open Access Article. Published on 07 June 2024. Downloaded on 6/20/2025 10:30:49 AM.
This article is licensed under a Creative Commons Attribution 3.0 Unported Licence.

8 G. Stoychev, A. Kirillova and L. Ionov, *Adv. Opt. Mater.*, 2019, **7**, 1900067.
9 J. Kolosnjaj-Tabi, L. Gibot, I. Fourquaux, M. Golzio and M. P. Rols, *Adv. Drug Delivery Rev.*, 2019, **138**, 56–67.
10 T. Manouras and M. Vamvakaki, *Polym. Chem.*, 2016, **8**, 74–96.
11 D. Schmaljohann, *Adv. Drug Delivery Rev.*, 2006, **58**, 1655–1670.
12 A. Zhang, K. Jung, A. Li, J. Liu and C. Boyer, *Prog. Polym. Sci.*, 2019, **99**, 101164.
13 N. K. Singh and D. S. Lee, *J. Controlled Release*, 2014, **193**, 214–227.
14 Y. Sun, J. Zhou, Q. Cheng, D. Lin, Q. Jiang, A. Dong, Z. Liang and L. Deng, *J. Appl. Polym. Sci.*, 2016, **133**, 43303.
15 L. J. Zhu, L. P. Zhu, Y. F. Zhao, B. K. Zhu and Y. Y. Xu, *J. Mater. Chem. A*, 2014, **2**, 15566–15574.
16 L. Li, Z. Xu, C. Zhang, R. Zhang, Z. Xu and A. K. Whittaker, *ACS Appl. Nano Mater.*, 2018, **1**, 5027–5034.
17 F. J. Xu, E. T. Kang and K. G. Neoh, *Biomaterials*, 2006, **27**, 2787–2797.
18 C. N. Kotanen, D. R. Janagam, R. Idziak, L. Rhym, R. Sullivan, A. M. Wilson, T. L. Lowe and A. Guiseppi-Elie, *Eur. Polym. J.*, 2015, **72**, 438–450.
19 Y. Li, S. P. Armes, X. Jin and S. Zhu, *Macromolecules*, 2003, **36**, 8268–8275.
20 J. I. Amalvy, E. J. Wanless, Y. Li, V. Michailidou, S. P. Armes and Y. Duccini, *Langmuir*, 2004, **20**, 8992–8999.
21 C. De las Heras Alarcón, S. Pennadam and C. Alexander, *Chem. Soc. Rev.*, 2005, **34**, 276–285.
22 R. París and I. Quijada-Garrido, *Eur. Polym. J.*, 2010, **46**, 2156–2163.
23 X. Zhou, X. Fan and C. He, *Macromolecules*, 2016, **49**, 4236–4244.
24 Y. Huang, P. Yong, Y. Chen, Y. Gao, W. Xu, Y. Lv, L. Yang, R. L. Reis, R. P. Pirraco and J. Chen, *RSC Adv.*, 2017, **7**, 28711–28722.
25 A. Roointan, J. Farzanfar, S. Mohammadi-Samani, A. Behzad-Behbahani and F. Farjadian, *Int. J. Pharm.*, 2018, **552**, 301–311.
26 J. Kopeĉek, *J. Polym. Sci., Part A: Polym. Chem.*, 2009, **47**, 5929–5946.
27 L. H. Hess, A. Lyuleeva, B. M. Blaschke, M. Sachsenhauser, M. Seifert, J. A. Garrido and F. Deubel, *ACS Appl. Mater. Interfaces*, 2014, **6**, 9705–9710.
28 Z. Jiang, X. Li, G. Yang, L. Cheng, B. Cai, Y. Yang and J. Dong, *Langmuir*, 2012, **28**, 7174–7181.
29 M. V. Risbud, A. A. Hardikar, S. V. Bhat and R. R. Bhonde, *J. Controlled Release*, 2000, **68**, 23–30.
30 M. Kurakula and G. K. Rao, *Eur. Polym. J.*, 2020, **136**, 109919.
31 J. E. Kennedy and C. L. Higginbotham, *Mater. Sci. Eng., C*, 2011, **31**, 246–251.
32 Q. V. Vo, T. L. B. Tram, N. T. Hoa, A. N. Au-Duong and A. Mechler, *Polym. Degrad. Stab.*, 2023, **216**, 110483.
33 G. Opiyo and J. Jin, *Eur. Polym. J.*, 2021, **159**, 110713.
34 X. Pan, X. Guo, B. Choi, A. Feng, X. Wei and S. H. Thang, *Polym. Chem.*, 2019, **10**, 2083–2090.
35 P. Van De Watering, N. J. Zuidam, M. J. Van Steenbergen, O. A. G. J. Van Der Houwen, W. J. M. Underberg and W. E. Hennink, *Macromolecules*, 1998, **31**, 8063–8068.
36 G. M. Iskander, L. E. Baker, D. E. Wiley and T. P. Davis, *Polymer*, 1998, **39**, 4165–4169.
37 Z. Hao, G. Li, K. Yang and Y. Cai, *Macromol. Rapid Commun.*, 2013, **34**, 411–416.
38 J. Deng, Y. Shi, W. Jiang, Y. Peng, L. Lu and Y. Cai, *Macromolecules*, 2008, **41**, 3007–3014.
39 V. J. Cunningham, M. J. Derry, L. A. Fielding, O. M. Musa and S. P. Armes, *Macromolecules*, 2016, **49**, 4520–4533.
40 R. R. Gibson, S. P. Armes, O. M. Musa and A. Fernyhough, *Polym. Chem.*, 2019, **10**, 1312–1323.
41 L. W. Teunissen, A. R. Kuzmyn, F. S. Ruggeri, M. M. J. Smulders and H. Zuilhof, *Adv. Mater. Interfaces*, 2022, **9**, 2101717.
42 L. W. Teunissen, M. M. J. Smulders and H. Zuilhof, *Langmuir*, 2023, **39**, 7613–7622.
43 J. Magalhaes, R. A. Sousa, J. F. Mano, R. L. Reis, F. J. Blanco and J. S. Román, *J. Biomed. Mater. Res., Part A*, 2013, **101A**, 157–166.
44 S. Jia, J. Fei, J. Deng, Y. Cai and J. Li, *Sens. Actuators, B*, 2009, **138**, 244–250.
45 S. Cheng, Y. Xue, Y. Lu, X. Li and J. Dong, *ACS Omega*, 2017, **2**, 105–112.
46 L. Wang, A. P. Constantinou, Y. Li and T. K. Georgiou, *Eur. Polym. J.*, 2024, **207**, 112810.
47 M. Elladiou and C. S. Patrickios, *Polym. Chem.*, 2012, **3**, 3228–3231.
48 M. Elladiou and C. S. Patrickios, *Macromolecules*, 2015, **48**, 7503–7512.
49 A. P. Constantinou, G. Patias, B. Somuncuoğlu, T. Brock, D. W. Lester, D. M. Haddleton and T. K. Georgiou, *Polym. Chem.*, 2021, **12**, 3522–3532.
50 D. Feldman and D. Feldman, *JPoSL*, 1984, **22**, 673–673.
51 M. G. Arafa, R. F. El-Kased and M. M. Elmazar, *Sci. Rep.*, 2018, **8**, 1–16.
52 K. Manokruang and D. S. Lee, *Macromol. Biosci.*, 2013, **13**, 1195–1203.
53 C. Gong, S. Shi, P. Dong, B. Kan, M. Gou, X. Wang, X. Li, F. Luo, X. Zhao, Y. Wei and Z. Qian, *Int. J. Pharm.*, 2009, **365**, 89–99.
54 M. A. Ward and T. K. Georgiou, *Polym. Chem.*, 2013, **4**, 1893–1902.
55 A. P. Constantinou, H. Zhao, C. M. McGilvery, A. E. Porter and T. K. Georgiou, *Polymers*, 2017, **9**, 31.
56 J. A. Pople, I. W. Hamley, J. P. A. Fairclough, A. J. Ryan, B. U. Komanschek, A. J. Gleeson, G. E. Yu and C. Booth, *Macromolecules*, 1997, **30**, 5721–5728.
57 G. E. Yu, H. Li, J. P. A. Fairclough, A. J. Ryan, N. McKeown, Z. Ali-Adib, C. Price and C. Booth, *Langmuir*, 1998, **14**, 5782–5788.
58 A. Kelarakis, V. Castelletto, C. Chaibundit, J. Fundin, V. Havredaki, I. W. Hamley and C. Booth, *Langmuir*, 2001, **17**, 4232–4239.

 This journal is © The Royal Society of Chemistry 2024

Open Access Article. Published on 07 June 2024. Downloaded on 6/20/2025 10:30:49 AM.
This article is licensed under a Creative Commons Attribution 3.0 Unported Licence.

59 J. Sun, Y. Peng, Y. Chen, Y. Liu, J. Deng, L. Lu and Y. Cai, *Macromolecules*, 2010, **43**, 4041–4049.
60 V. Bütün, S. P. Armes and N. C. Billingham, *Polymer*, 2001, **42**, 5993–6008.
61 V. J. Cunningham, Y. Ning, S. P. Armes and O. M. Musa, *Polymer*, 2016, **106**, 189–199.
62 V. J. Cunningham, S. P. Armes and O. M. Musa, *Polym. Chem.*, 2016, **7**, 1882–1891.
63 H. Lee, S. H. Son, R. Sharma and Y. Y. Won, *J. Phys. Chem. B*, 2011, **115**, 844–860.
64 J. C. P. De Souza, A. F. Naves and F. H. Florenzano, *Colloid Polym. Sci.*, 2012, **290**, 1285–1291.
65 D. Fournier, R. Hoogenboom, H. M. L. Thijs, R. M. Paulus and U. S. Schubert, *Macromolecules*, 2007, **40**, 915–920.
66 M. A. Ward and T. K. Georgiou, *J. Polym. Sci., Part A: Polym. Chem.*, 2010, **48**, 775–783.
67 P. Liu, L. Xiang, Q. Tan, H. Tang and H. Zhang, *Polym. Chem.*, 2013, **4**, 1068–1076.
68 Y. Cho, L. B. Sagle, S. Iimura, Y. Zhang, J. Kherb, A. Chilkoti, J. M. Scholtz and P. S. Cremer, *J. Am. Chem. Soc.*, 2009, **131**, 15188–15193.
69 P. Kujawa and F. M. Winnik, *Macromolecules*, 2001, **34**, 4130–4135.
70 B. Sun, Y. Lin, P. Wu and H. W. Siesler, *Macromolecules*, 2008, **41**, 1512–1520.
71 X. Wang and C. Wu, *Macromolecules*, 1999, **32**, 4299–4301.
72 X. Jiang, G. Zhang, R. Narain and S. Liu, *Langmuir*, 2009, **25**, 2046–2054.
73 X. Jiang, G. Zhang, R. Narain and S. Liu, *Soft Matter*, 2009, **5**, 1530–1538.
74 W. Zhang, X. Jiang, Z. He, D. Xiong, P. Zheng, Y. An and L. Shi, *Polymer*, 2006, **47**, 8203–8209.
75 S. Liu, J. V. M. Weaver, Y. Tang, N. C. Billingham, S. P. Armes and K. Tribe, *Macromolecules*, 2002, **35**, 6121–6131.
76 M. Vamvakaki and C. S. Patrickios, *Chem. Mater.*, 2002, **14**, 1630–1638.
77 C. Yang, J. Xiao, W. Xiao, W. Lin, J. Chen, Q. Chen, L. Zhang, C. Zhang and J. Guo, *RSC Adv.*, 2017, **7**, 27564–27573.
78 H. Yang, J. Guo, R. Tong, C. Yang and J. K. Chen, *Polymers*, 2018, **10**, 443.
79 Y. Xing, J. Peng, K. Xu, S. Gao, X. Gui, S. Liang, L. Sun and M. Chen, *Phys. Chem. Chem. Phys.*, 2017, **19**, 23024–23033.
80 C. Wu, A. Ying and S. Ren, *Colloid Polym. Sci.*, 2013, **291**, 827–834.
81 D. Laage, T. Elsaesser and J. T. Hynes, *Chem. Rev.*, 2017, **117**, 10694–10725.
82 S. Wang, G. N. Nawale, O. P. Oommen, J. Hilborn and O. P. Varghese, *Polym. Chem.*, 2019, **10**, 4322–4327.
83 J. Y. Shin, Y. H. Yeo, J. E. Jeong, S. A. Park and W. H. Park, *Carbohydr. Polym.*, 2020, **238**, 116192.
84 A. P. Constantinou, L. Wang, S. Wang and T. K. Georgiou, *Polym. Chem.*, 2023, **14**, 223–247.
85 M. Kunitz, *J. Gen. Physiol.*, 1928, **12**, 289–312.
86 R. Kocen, M. Gasik, A. Gantar and S. Novak, *Biomed. Mater.*, 2017, **12**, 025004.
87 S. K. H. Gulrez, S. Al-Assaf and G. O. Phillips, *Progress in molecular and environmental bioengineering-from analysis and modeling to technology applications*, InTech: Rijeka, Croatia, 2011.